A Study on Arctic Sea Ice Dynamics Using the Continuous Spin Ising Model

Ellen Wang[1 a)]

AFFILIATIONS

[1] Horace Mann School, Bronx, NY, USA

[a)] Author to whom correspondence should be addressed: ellen.ls.wang@gmail.com

Abstract

The Ising model, initially proposed about 100 years ago to explain ferromagnetism and phase transitions, has become a central pillar of statistical physics and a powerful tool for diverse applications in other fields including environmental studies. In this paper, we introduce continuous spin values between −1 and +1 to a two-dimensional Ising model and utilize the generalized Ising lattice to simulate the dynamics of sea ice/water transition for a large area of 1500km by 1500km in the Arctic region. The simulation process follows the Metropolis-Hastings algorithm and incorporates an innovative factor to account for the inertia of spin value changes. Using the sea ice concentration data collected by the National Snow and Ice Data Center, our results exhibit striking similarity between the simulated and the observed ice melting and freezing dynamics, and two numerical measures from the simulation—the ice coverage percentage and the ice extent—match closely with the data statistics. Moreover, the model's best-fit parameters demonstrate the substantial impact of the external forces, which can be further enriched and linked to the environmental factors in other climate change research.

Keywords: *Ising model, continuous spin, Metropolis-Hastings algorithm, phase transition, Arctic sea ice, climate change*

I. Introduction

This study models Arctic Sea Ice dynamics at a large scale by innovating on the centennial Ising model (IM). The rapid Arctic sea ice loss observed in recent years [1] [2] and the hottest year 2023 recorded on the earth [3] make our study particularly meaningful. Upon the classical binary-spin Ising [4] [5] setup, we first introduce the continuous spin values [6] [7] and then enhance the model by incorporating a novel inertia factor. The simulated evolution of ice/water phase transition follows the Metropolis-Hastings [8] Monte Carlo process governed by this generalized model. The Arctic sea ice images collected by the National Snow and Ice Data Center [9] serve as the inputs into our model, which outputs the best-fit Ising parameters and the simulated sea ice configurations. Our analyses of the simulated configurations and the numeric measures calculated from the simulation results validate the strong explanatory power of our generalized model in sea ice studies. After a brief review on Ising literature and an introduction of the significance of Arctic sea ice, Section II lays out the theoretical framework of our generalized Ising model, Section III describes the Arctic sea ice data, Section IV illustrates the computational setup, and Section V presents the results and analysis, followed by final discussions in Section VI.

A. Ising model

The classical Ising model is the backbone of this study. It was first formalized by physicists Ernst Ising and Wilhelm Lenz to explain the equilibrium and phase transition in magnetic systems. The one-dimensional (1-D) IM was solved by Ising in his 1924 thesis [4] [5] [10], which proves the non-existence of phase transition in the 1-D IM. In 1944, Lars Onsager [11] was able to solve the two-dimensional (2-D) square-lattice IM analytically. Contradictory to the 1-D case, Onsager identified that there exists a critical temperature $T_c = 2.27\ J/k_B$ when the phase transition happens in a 2-D IM. Later studies of IM in higher dimensions have been closely associated with various developments in advanced 20th-century physics and mathematical theories, including the transfer-matrix method [12] [13], quantum field theory [14], mean-field theory [15], etc.

Over the years, the IM has found wide success beyond physics. Specifically, the Kinetic IM [15] [16] [17], built upon the equilibrium version, has been proposed to analyze biology, environmental science, machine learning [18] [19], social science, and economic and financial systems. These applications are widely implemented as a discrete time Markov chain of the spin lattice, with spin interactions bounded to finite distance. In biology and neuroscience, IM applications include but are not limited to the condensation of DNA [20], genetics [21], neural networks [22] [23], neuron spike [24], neuron activity in cell assemblies [25], and ligands to receptors binding in cells [26]. In environmental science, the IM has been employed to investigate land pattern dynamics [27] [28]. Recently, Ma, Sudakov, Strong and Golden have successfully used the 2-D IM to capture the essential mechanism of the ice melt ponds equilibrium configuration [29]. In social science, economics, and finance, the IM has been applied to research in urban segregation [30], crisis study [31], stability of money [32], etc.

B. Arctic sea ice

The reversible phase transition between water and ice makes the IM a great tool to study the dynamics of a surface region with the co-existence of both states. In this paper, we apply a 2-D IM lattice to study

the dynamics of Arctic sea ice melting and freezing cycles, a major climate change indicator that is of significant environmental, economic, and social significance [33].

Sea ice is undoubtedly an integral part of the Arctic Ocean and the earth [33]. In the dark winter months, ice covers almost the entirety of the Arctic Ocean, and the ice extent—defined as the percentage of the areas that are covered by at least 15% ice—and the ice thickness typically reaches its peak around March. Starting in late spring, ice melting gradually exceeds water freezing due to higher temperatures and longer hours of sunlight exposure. Sea ice typically reaches the minimum extent and thickness in mid-September, when ice coverage can drop to under half of the winter maximum [34]. After mid-September, sea water freezing starts to exceed ice melting, so ice coverage expands. This cycle repeats annually.

Albedo, the percentage of incident light reflected from the surface of the earth, is highly dependent on the ice extent [35]. Light-colored ice or snow reflects more light than blue-colored liquid water; therefore, ice is essential to keeping the Arctic at a cooler temperature and subsequently maintaining the energy balance around the globe. If the energy balance is broken, as ice decline has been detected in recent years, the ice-albedo feedback loop effect may occur, i.e., less reflection and more absorption of solar energy, leading to even more ice loss and further global warming. Moreover, the Arctic ecosystem is directly impacted by the change in sea ice coverage, which, for instance, threatens the lives of polar bears and walruses who rely on sea ice for hunting and breeding [36].

Data recorded by the National Aeronautics and Space Administration (NASA) and the National Snow and Ice Data Center (NSIDC) since 1979 has shown substantial declines in both ice extent and thickness in the Arctic, despite the year-over-year fluctuations in either direction. The lowest Arctic sea ice extent was observed in September of 2012 [1] [37]; between 2013 and 2022, the ice extent was higher than the 2012 minimum, but still much lower than the average of the past four decades. July 2023 was reported as the hottest month of the earth on record [38], and 2023 the hottest year by a significant margin [3] [39]. Some questions then come to us naturally: how does the Artic sea ice extent in 2023 compare to the 2012 level? And can our model simulations closely match the observations in the real data? These questions will be addressed in Section V.D.

II. Theoretical framework

A. Classical Ising model

The system described by an IM is a set of lattice sites, each having a spin that interacts with its neighbors. The Hamiltonian function [4] [5] [10] for the lattice σ in a standard IM is given as

$$H(\sigma) = -\sum_{<i,j>} J_{ij}\sigma_i\sigma_j - \sum_i B_i\sigma_i. \quad (1)$$

where σ_i represents the spin variables at site i and takes the value of +1 or -1; J_{ij} represents the interaction between sites i and j and can take positive values for ferromagnetic and paramagnetic materials, or negative for antiferromagnetic materials; B_i captures the interaction between the external field and site i. i and j range across the full lattice, which can be one, two or higher dimensions, and $<i, j>$ represents pairs of spins at sites i and j that interact with each other. In a simple setup, each spin only interacts with its nearest neighbors, so $<i, j>$ sums over adjacent sites only. For example, in a

simple 2-D IM, each spin interacts only with the sites positioned immediately left, right, above, and below.

In statistical physics, the configuration probability of lattice σ follows the Boltzmann distribution [40]:

$$P_\beta(\sigma) = \frac{e^{-\beta H(\sigma)}}{Z_\beta}, \tag{2}$$

where Z_β is the partition function:

$$Z_\beta = \sum_\sigma e^{-\beta H(\sigma)}, \tag{3}$$

and

$$\beta = (k_B T)^{-1}. \tag{4}$$

β is the inverse temperature; k_B is the Boltzmann constant; T is the IM temperature, which differentiates from the ambient temperature discussed later.

The evolution of the kinetic IM runs through a series of spin flips over the lattice. The probability of each flip depends on whether it increases or reduces the Hamiltonian of the system. Mathematically, the probability is determined by $\min(1, e^{-\beta(H_\nu - H_\mu)})$ [41], where H_ν and H_μ represent the Hamiltonian of the system before and after the flip. We can easily see that higher IM temperatures lead to greater thermal fluctuations and larger variances in the spin value distribution, while lower IM temperatures result in fewer fluctuations.

B. Continuous spin Ising model

Most of the Ising literature cited in earlier sections [5] [10] [21] [28] [29] focus on binary values of the spins, i.e., σ_i taking values of +1 or -1 only. However, the sea ice data for each location takes varying values between 0 and 1 that represent the percentage of ice coverage. Therefore, we generalize the IM to allow for continuous spin values that can take any real number between -1 and +1. This generalization enables the IM to examine more realistic systems, but also adds a high degree of complexity to the mathematical solutions. Past research has studied phase transitions and critical behaviors of the continuous IM [6] [7]. Recently, an IM with variable power-law spin strengths is studied with its rich phase diagrams [42].

The Hamiltonian function of the continuous spin IM is represented by the same Equation (1). However, σ_i now takes continuous values between $+1$ and -1; $-J_{ij}\sigma_i\sigma_j$ reaches the minimum energy state if $\sigma_i = \sigma_j = +1$, or $\sigma_i = \sigma_j = -1$, as the energy of any other value pair is higher. The highest energy is observed when $\sigma_i = +1$, $\sigma_j = -1$, or vice versa. This numeric feature works ideally for an ice/water lattice: the most stable low energy state is either 100% water or ice across two adjacent locations, whereas full ice next to full water displays the most unstable high energy state.

C. Monte Carlo simulation and inertia factor

The introduction of the continuous spins also adds to the complexity of the Monte Carlo (MC) simulation of the Ising lattice. In the classical binary-spin IM, σ_i can only flip to $-\sigma_i$, and therefore the absolute value of the change is always 2 no matter if the flip goes from -1 to +1 or vice versa. In a continuous spin IM, the challenge of determining a post-flip spin value nevertheless arises. In our approach, this new spin value is implemented through a random number σ'_i uniformly distributed between -1 and +1, which will be explained in greater details in Section IV.D. Moreover, we incorporate an innovative inertia factor *I*, and the probability of each flip is determined by

$$P_{flip} = \min\left(1, e^{-\beta(H_\nu - H_\mu + I|\sigma'_i - \sigma_i|)}\right), \tag{5}$$

where σ_i represents the original spin value before the change, σ'_i the new attempted value, and H_ν and H_μ the system Hamiltonian before and after as described in Equation (1) and Section II.A.

The newly added $-I|\sigma'_i - \sigma_i|$ accounts for the energy needed to overcome the inertia of the spin change, and *I* is an IM parameter to be fitted. Intuitively, this term represents the natural resistance to any state change, and can also be thought of as an analog to the latent heat needed for the ice/water phase transition in classical thermodynamics. Motivated by the fact that the total energy change for water/ice phase transition at constant temperature and pressure is proportional to mass, we choose a linear functional form for the inertia term as the simplest and most sensible assumption. Therefore, the total energy change required for a spin flip is $\Delta E = H_\nu - H_\mu + I|\sigma'_i - \sigma_i|$, which consists of two parts: the system Hamiltonian change plus the inertia term. The probability of spin value change follows the Boltzmann distribution as Equation (5).

Here is an example to illustrate the inertia effect. Starting with an initial spin value of 0.8, a flip to either 0.7 or 0.6 may result in the same system Hamiltonian. However, we differentiate these two new states by assigning higher probability for the flip to 0.7 because of the smaller spin change. In Equation (5), $-I|\sigma'_i - \sigma_i|$ influences the distribution of the new spin values, and in practice, it significantly improves the simulation results to better match the observations.

In summary, we introduce a novel inertia factor to the continuous spin IM. These mathematical additions prepare us to study real-world Arctic sea ice dynamics while keeping the computational complexity tractable.

III. Data description

Our study uses the "Near-Real-Time DMSP SSMIS Daily Polar Gridded Sea Ice Concentrations" (NRTSI) dataset [9] collected by the National Snow and Ice Data Center (NSIDC), which captures daily sea ice concentrations for both the Northen and Southern Hemispheres. The Special Sensor Microwave Imager/Sounder (SSMIS) on the NANA Defense Meteorological Satellite Program (DMSP) satellites acquires the near-real-time passive microwave brightness temperatures, which are inputted into the NRTSI dataset using the NASA Team algorithm to generate the sea ice concentrations.

The NRTSI files are in netCDF format. Each file of the Arctic region contains a lattice of 448 rows by 304 columns, covering a large earth surface area with the north pole at the center. Each grid cell

represents an area of approximately 25 kilometers by 25 kilometers. The value for each grid cell is an integer from 0 to 250 that indicates the fractional ice coverage scaled by 250, with 0 indicating 0% ice concentration and 250 for 100% ice concentration. The image of part of the NRTSI file on Sept 16th, 2022 is illustrated in Figure 1(a). In the map, white represents ice, blue represents water, and gray represents land. The exact location of the north pole is covered by a gray circular mask because of the limitation of the satellite sensor measurement caused by the orbit inclination and instrument swath. The red oval marks the Canadian Arctic Archipelago area with the thickest ice [43], which is worth of some discussions later in the paper.

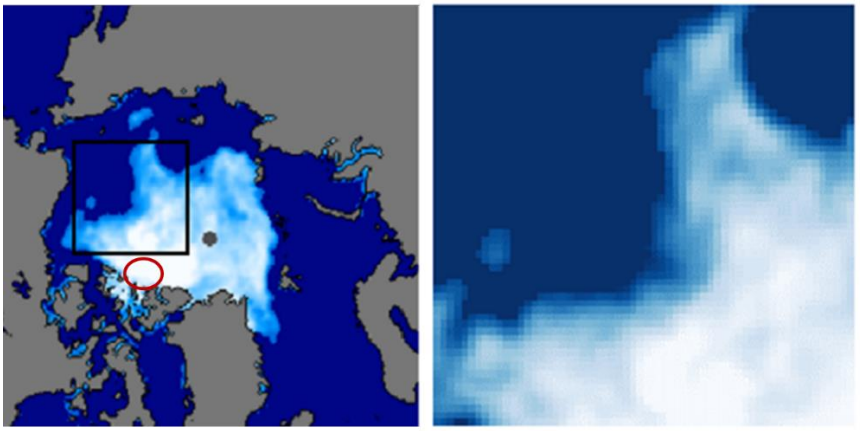

Figure 1: (a) Part of the NRTSI data on Sept 16th, 2022, where the black square marks the focus area for this study and red oval the Canadian Arctic Archipelago area with the thickest ice [43]; (b) A zoom-in view of the focus area, a 60x60 square lattice covering approximately 2.25 million square kilometers.

For this research paper, we focus on studying a specific geographic region bounded by the black square in Figure 1(a), ranging from the East Siberian Sea (to the top of the box) and the Beaufort Sea (to the left) to near the polar point; a zoom-in image of this focus area is shown in Figure 1(b) . This large square area is unobstructed by land or the north pole mask, making it ideal for the IM lattice setup. This area corresponds to 60 rows and 60 columns in the data file, covering approximately 1500km x 1500km, or about 2.25 million square kilometers.

IV. Ising lattice and simulation setup

The methodology of our study on sea ice dynamics is outlined as follows: We first normalize the NRSTI data to a continuous Ising lattice, carefully choose the simulation periods, and set up the Ising parameters (J, B, I) to be fitted. Then given the initial lattice of each simulation period, we run the Metropolis MC simulation based on the values of (J, B, I) to generate a final state of the Ising lattice for this period. The full Metropolis simulation procedure is passed into a numeric optimizer to find the best-fit Ising parameters so that the simulated final Ising lattice matches the observed NRSTI data as closely as possible.

A. Ising lattice

We start with a transformation of the NRTSI data of the focus region shown in Figure 1 (b) to the Ising-style data. A simple linear mapping is applied to convert integers from 0 to 250 to real numbers from -1 to +1. -1 indicates that a location cell is 100% ice, +1 indicates 100% water, and 0 indicates 50%/50% coverage of water/ice. Each cell covers 25km x 25km of the total 1500km x 1500km focus region, and therefore a 60x60 matrix is initialized for the 2-D IM lattice in our study.

B. Simulation periods

Figure 2 (a) and (b) display an example of the initial and the final target states of an IM lattice simulation run. The simulation periods are chosen to be consistently half a month apart, for example, Sept 16th, 2022 in Figure 2 (a) and Oct 1st, 2022 in Figure 2 (b). This semi-monthly frequency is chosen to balance two considerations. First, the period is sufficiently long to allow for sizable differentiation in the ice/water configurations between the start and the end dates; second, the period is not too long and allows the IM simulation to mimic the daily ice/water evolution on the interim dates between the start and the end, which is to be illustrated in Section V.B.

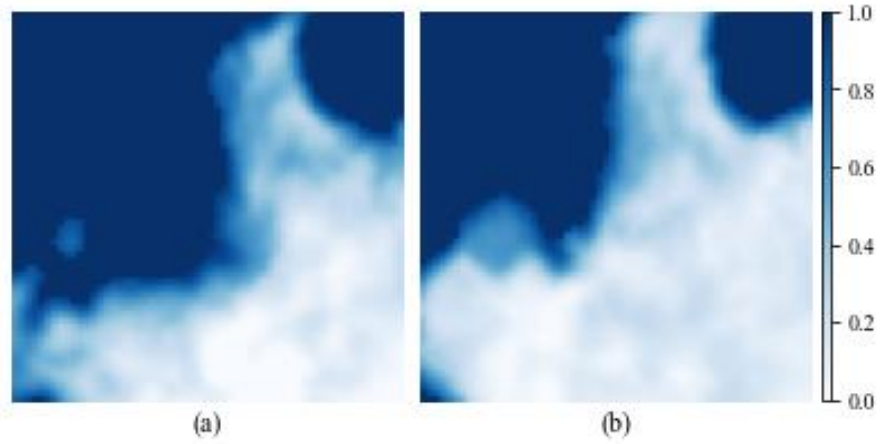

Figure 2: The initial and the final target states of an IM lattice simulation run. (a) shows the actual configuration observed in our focus area on Sept 16th, 2022 and (b) on Oct 1st, 2022. Each full simulation period is half a month. Blue color indicates water; white indicates ice. The darker the color of each cell, the higher the water concentration and the lower the ice coverage, as shown by the color scale on the right.

C. Ising model parameters

In the IM Hamiltonian function, i.e., Equation (1), we set the following:

- σ_i is a real number between -1 and +1 for any cell i in our focus area.
- $<i, j>$ sums over four adjacent cells positioned immediately left, right, above, and below.
- J_{ij} is set to be constant within each simulation period across all cells.

- B_i is set to be time-invariant within each simulation period. However, in order to capture the variations in the external forces due to the environmental differences across geographic locations, B_i is set to be a linear function of x_i and y_i coordinates (the row and the column of cell i in the Ising lattice respectively), i.e., $B_i = B_0 + B_x(x_i - x_0) + B_y(y_i - y_0)$, where B_0 is the value of B at the lattice center with coordinates x_0 and y_0 .
- I, the inertia factor, is set to be constant within each simulation period.
- β, the inverse Boltzmann temperature, is set to 1. In this study, what matters is the relative magnitudes of (J, B_0, B_x, B_y, I) instead of their individual absolute values, so we can set β to 1 without loss of generality. A similar approach has been taken in other kinetic Ising model research [28].

D. Metropolis simulation steps

Various MC methods have been developed for the IM simulation. Among them the most widely used are the Glauber dynamics [44] and the Metropolis-Hasting algorithm [8]. In our study, we follow the latter for the MC simulation of the IM lattice evolution. As described in Section II.C, an inertia factor is introduced into our model and the generalized Metropolis-Hastings MC steps are listed below:

1. Select cell i at random from the 2-D lattice of the focus area. Let the spin value of this cell be σ_i.
2. Generate another uniform random variable σ'_i between -1 and +1.
3. Compute the energy change $\Delta H_i = H_\nu - H_\mu$ from σ_i to σ'_i.
4. Compute the energy $I|\sigma'_i - \sigma_i|$ to overcome the inertia of changing the spin value at i.
5. Compute the total energy change $\Delta E = \Delta H_i + I|\sigma'_i - \sigma_i|$.
6. (a) If ΔE is negative, the energy change is favorable since the energy is reduced. The spin value change is therefore accepted to σ'_i.
   (b) If ΔE is positive, the probability of the spin flip is determined by the Boltzmann distribution. In this case, another uniform random variable r between 0 and 1 is generated. If r is less than $P = e^{-\beta \Delta E}$, the spin value change is accepted; otherwise, the change is rejected and the spin value at i stays at σ_i.

For each semi-monthly simulation period, we repeat the above MC steps 50,000 times. As the lattice of our focus area has 3,600 cells, this repetition allows for approximately 14 flip tries for each cell, or roughly once per day. This specific repetition number is chosen by taking into account the computational complexity of the algorithm and also making sure that each cell of the Ising lattice gets sufficient attempts to be changed. Other choices of the repetition number can be considered, which may result in different fitted parameter values. What is important is to ensure the number of repetitions for each period proportional to its duration, so the time unit of each Metropolis step is the same across the full simulation process [28].

E. Dual annealing optimization

As described in the previous section, the Ising parameters (J, B_0, B_x, B_y, I) dictate the sea ice evolution process in the Metropolis MC simulations, and therefore different parameter regimes shall lead to varying final states. With the goal to match the observed final state lattice configuration as

closely as possible upon the completion of the simulations, we measure the similarity between the observed and the simulated final lattice configurations by the sum of the absolute spin value differentials across the lattice. Mathematically, this is the Manhattan distance (as opposed to the more commonly used Euclidean distance) between the observed and the simulated matrices. We then fit the values of parameters (J, B_0, B_x, B_y, I) to maximize of the similarity measure, i.e., to minimize the sum of the absolute spin value differentials. The minimization is done with the dual annealing optimization method, which combines classical simulated annealing with a local search to achieve the global minimization solution [45] [46]. Description of the dual annealing method can be found in the Python SciPy package.

V. Results

We employ the continuous spin IM to simulate the dynamics of the sea ice/water transition for the focus Arctic Sea area. Thanks to the NRTSI data, we can conduct the simulation for every year in the past four decades.

A. Simulation results for 2022

Figure 3 shows the actual semi-monthly sea ice images in our focus area from June 16th, 2022 to Jan 1st, 2023. As can be seen, the melting cycle starts from June 16th and goes until Sept 16th, and the freezing cycle from Sept 16th to year end. Prior to June 16th, the region is almost fully covered by ice, so the IM simulation will be trivial. This is why we set the simulation start date on June 16th of each year. During the period of June 16th to Dec 16th, every successive image shows considerable ice coverage difference from the previous date while retaining certain core features. This semi-monthly frequency choice allows our IM simulation to capture the essence of the evolution dynamics without overfitting the model.

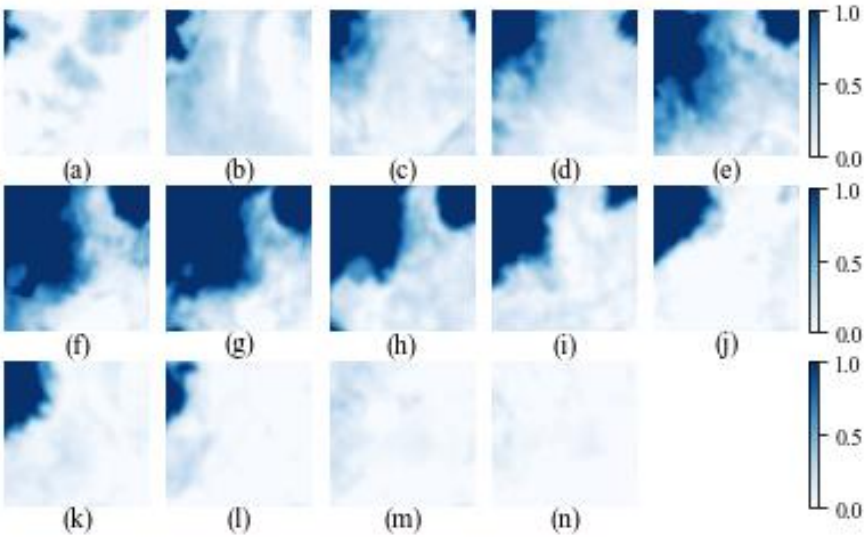

Figure 3: The actual semi-monthly sea ice evolution in our focus area in 2022: (a) June 16th, (b) July 1st, (c) July 16th, (d) Aug 1st, (e) Aug 16th, (f) Sept 1st, (g) Sept 16th, (h) Oct 1st, (i) Oct 16th, (j) Nov 1st, (k) Nov 16th, (l) Dec 1st, (m) Dec 16th, 2022, and (n) Jan 1st, 2023.

The best-fit Ising parameters (J, B_0, B_x, B_y, I) for each simulation period in 2022 are shown in Table 1. The spin interaction coefficient J and the inertia factor I are relatively stable; intuitively, the strength of such interactions does not change much across different time periods. Moreover, J remains positive across all periods, confirming that adjacent cells are inclined to maintain values of the same sign, i.e., the area surrounding ice will be more likely to freeze, and that surrounding water will tend to melt. In this sense, the ice/water system displays the feature of ferromagnetism/paramagnetism instead of antiferromagnetism.

On the other hand, the external force parameters B_0, B_x, and B_y display large variations across different time periods. In particular, the average force B_0 is positive from June 1st to Sept 16th but turns negative afterwards, which can be explained by the seasonal ambient temperature as the dominant external factor for ice/water dynamics. Ambient temperature is not the only factor, though. Arctic temperature normally peaks in July/August while B_0 remains positive and ice melting continues through mid-September. This lag effect could be explained by other environmental effects such as albedo or jet streams but is beyond the scope of this study.

The values of B_x and B_y are mostly negative due to the geographic distribution of ice coverage. For our Ising lattice representing the focus area, x coordinates corresponding to the rows of the lattice increase from top to bottom; y coordinates for the columns increase from left to right. Interestingly, ice coverage near the bottom of our area, the Canadian Arctic Archipelago marked by the red oval in Figure 1, is much thicker than elsewhere including the north pole (the gray circular mask). In fact, many scientists believe this region will have the last piece of ice standing in the Arctic if the Blue Ocean Event happens [43]. As the lower part of the focus area tends to have greater ice coverage, B_x is mostly negative, except for very few periods when the ice coverage remains relatively unchanged. B_y is less negative, as the impact of the geographic location along the y direction is less pronounced than that of x because the ice at the north pole is thinner than in Archipelago, which mitigates the impact of the y coordinate of a cell. In addition, the values of B_x and B_y exhibit greater fluctuations than other parameters, indicating that our simplified linear functional form of $B_i = B_0 +$

$B_x(x_i - x_0) + B_y(y_i - y_0)$ is far from perfectly modeling the full effect of external fields; it can be further enriched by linking to actual geographical and environmental factors to enhance the power of the Ising model, which is left for our future research.

	6/16 to 7/1	7/1 to 7/16	7/16 to 8/1	8/1 to 8/16	8/16 to 9/1	9/1 to 9/16	9/16 to 10/1	10/1 to 10/16	10/16 to 11/1	11/1 to 11/16	11/16 to 12/1	12/1 to 12/16	12/16 to 1/1/2023
J	2.3	2.6	2.3	2.4	2.7	2.3	2.6	2.7	2.6	2.5	2.3	2.7	2.7
B_0	7.0	2.0	6.5	9.1	4.3	3.6	-12.6	-12.7	-14.9	-9.6	-15.0	-13.1	-14.4
B_x	0.2	-9.7	-5.5	3.7	-7.5	-8.2	-10.0	-6.1	-8.5	9.7	-1.9	-0.8	-3.1
B_y	-10.0	3.0	3.7	1.0	-6.4	2.9	0.1	-8.4	-5.6	-10.0	-5.9	5.4	-8.0
I	10.3	9.1	11.0	10.8	10.7	10.9	10.6	9.3	9.4	10.4	9.1	10.9	10.8

Table 1: The best-fit Ising parameters for the 2022 sea ice evolution.

The simulated sea ice images for each 2022 period are shown in Figure 4 utilizing the best-fit Ising parameters in Table 1. These images exhibit excellent similarity to Figure 3, demonstrating the strong explanatory power of our Ising model. Nevertheless, upon close inspection, the images in Figure 3and Figure 4 do reveal discrepancies, especially as shown in images ((e) for Aug 16th, (h) Oct 1st, and (i) Oct 16th, 2022 respectively, where the ice image display significant irregularity compared to the prior period. While an IM with simple parameterization encounters difficulties in describing these local irregularities, it is feasible to include a richer set of parameters or to employ more complicated parametric functional forms at the potential cost of overfitting. In this paper, we keep our Ising model tractable and accept these local discrepancies.

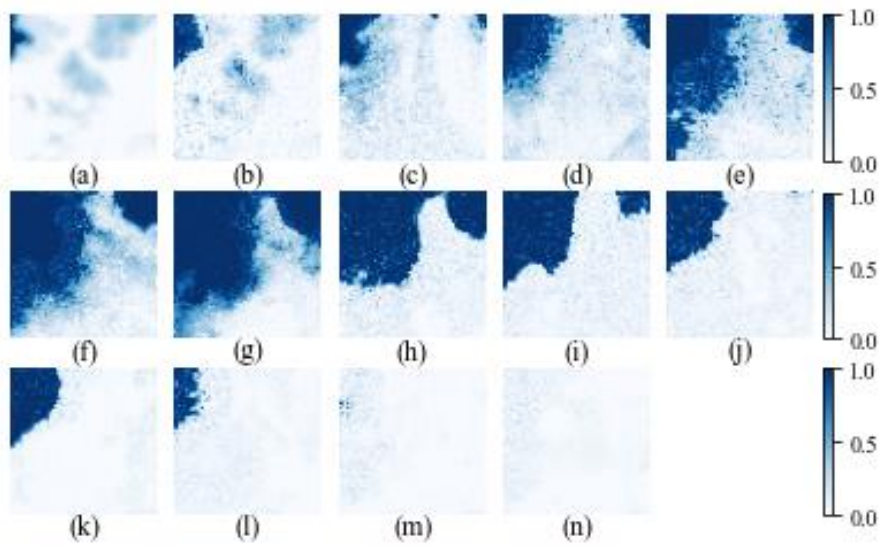

Figure 4: The simulated semi-monthly sea ice evolution in our focus area in 2022. (a) is the actual image on June 16th, 2022 as the start state; (b) - (n) are simulated images on (b) July 1st, (c) July 16th, (d) Aug 1st, (e) Aug 16th, (f) Sept 1st, (g) Sept 16th, (h) Oct 1st, (i) Oct 16th, (j) Nov 1st, (k) Nov 16th, (l) Dec 1st, (m) Dec 16th, and (n) Jan 1st, 2023.

To quantify the similarity between the IM simulated configurations and the observed images, the absolute difference in ice coverages across the entire focus area for each of the simulation period in Figure 3 and Figure 4 are calculated; the results are illustrated as the heatmaps in Figure 5 (a) – (n),

where light yellow color indicates that the actual and the simulated images match well, whereas red patches are associated with the locations that display large discrepancy. The heatmaps are very revealing: the red patches are consistently small and mostly appear around the boundaries between water and ice, implying that most of the discrepancy between the simulated and actual images happens around these border areas. This is not surprising: the IM needs improvement to perfectly model these boundary granularities, but it does have strong capability to capture the overall patterns.

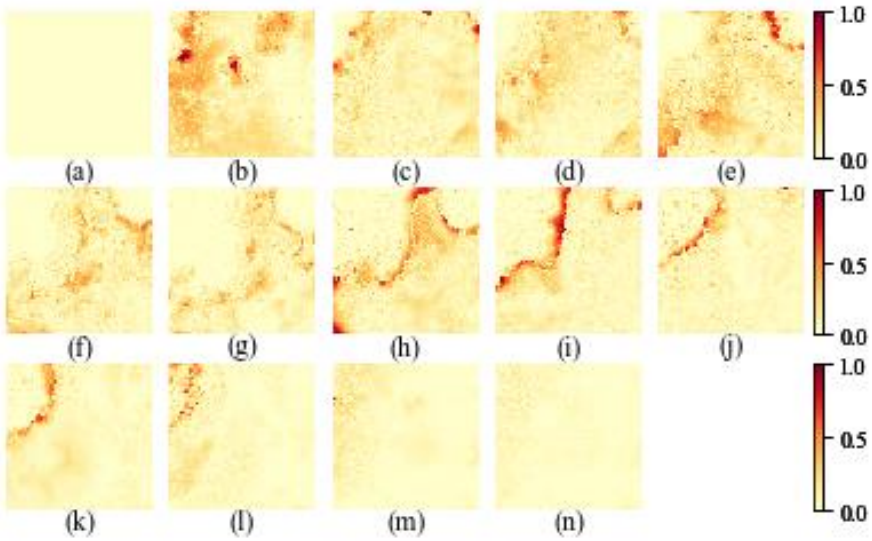

Figure 5: Heatmaps illustrating the absolute difference (between 0 and 1) in ice coverages between Figure 3 and Figure 4 for each semi-monthly period, from (a) June. 16th, 2022 to (n) Jan. 1st, 2023. Yellow color indicates a good match and red a large difference, as shown by the scale on the right.

Furthermore, we compute two key numerical measures for our focus area: the ice coverage percentage, i.e., the average ice coverages over the lattice, and the ice extent, i.e., the percentage of areas covered by at least 15% ice. Figure 6 compares the actual and the simulated measures; as anticipated, we see an excellent match in both figures as a result of the superior explanatory power of our IM, despite marginal but non-trivial discrepancy. It is interesting to note that the simulated ice coverage percentage is mostly slightly higher than the actual measure, but the simulated ice extent is slightly lower than the actual, a pattern that can be further investigated in future research.

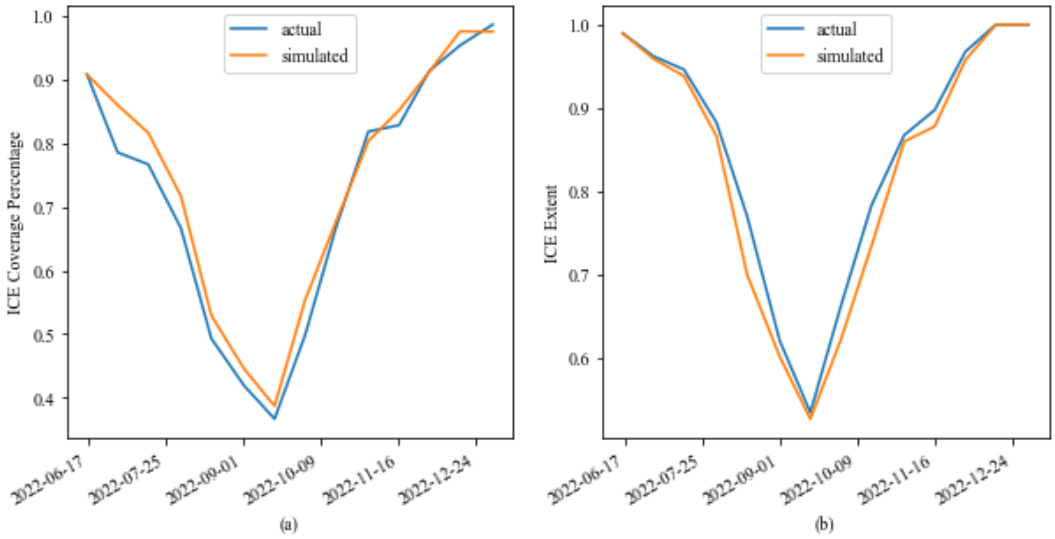

Figure 6: (a) The ice coverage percentage (the average of ice coverages) in our focus area from June 16th, 2022 to Jan 1st, 2023; (b) The sea ice extent (the percentage of areas with at least 15% ice coverage) for the same period. Blue curves are the actual measures from the NRTSI data; orange ones show the IM simulation results.

B. Daily sea ice evolution in 2022

Do our semi-monthly IM simulation results match the actual sea ice dynamics on a shorter time scale? To answer this question, we utilize the semi-monthly Ising parameters in Table 1 to simulate the daily evolution in 2022. Two periods, a melting period from Aug 16th to Sept 1st, 2022, and a freezing period from Oct 16th to Nov 1st, 2022, are simulated day-by-day for this experiment. The results, with comparisons between the actual and the simulated daily ice evolution, are shown in Figure 7, Figure 8, Figure 9, and Figure 10 respectively. The comparisons exhibit excellent similarity across all the daily images in both periods, confirming that our IM preserves the ice/water dynamics on a shorter time scale.

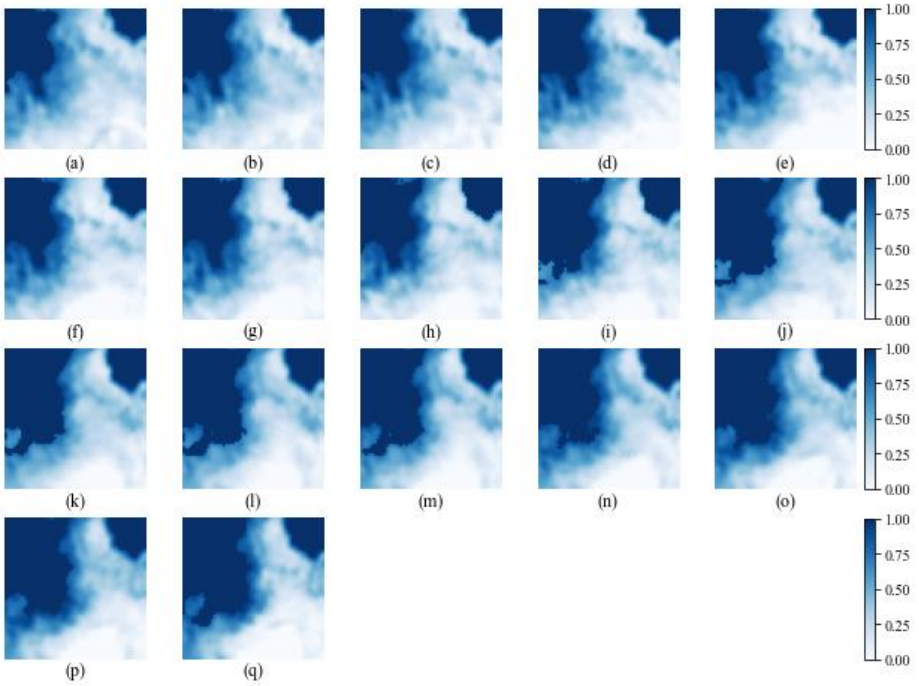

Figure 7: The actual daily sea ice evolution in our focus area during a melting cycle from (a) Aug 16th to (q) Sept 1st, 2022.

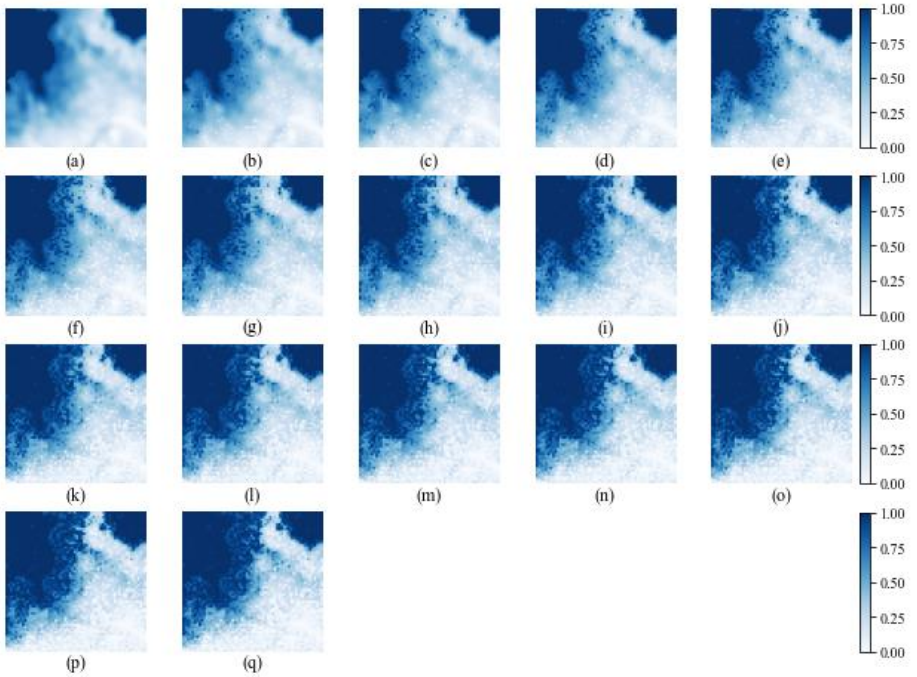

Figure 8: The simulated daily sea ice evolution , based on the semi-monthly Ising parameters, in our focus area during a melting cycle from (a) Aug 16th to (q) Sept 1st, 2022.

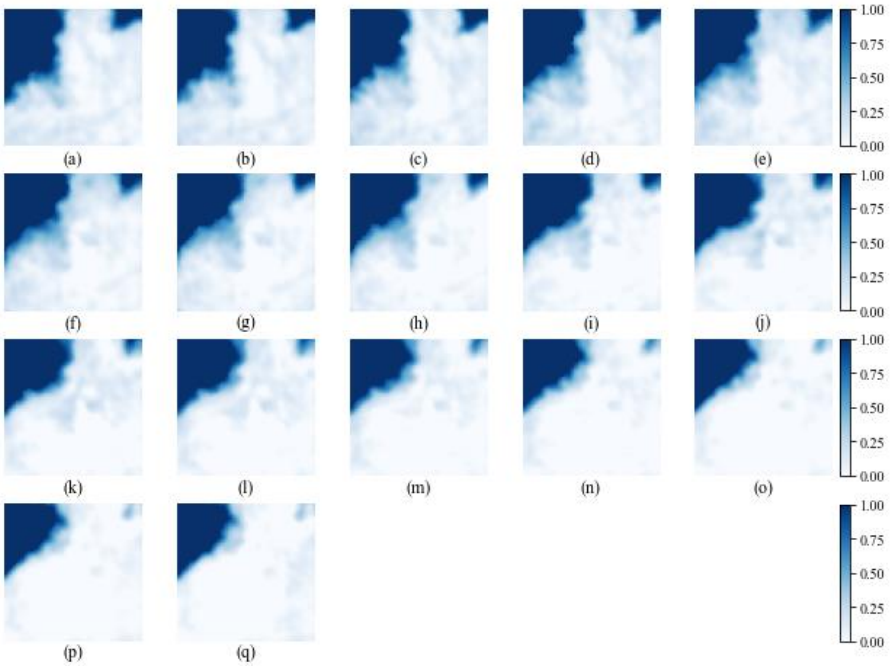

Figure 9: The actual daily sea ice evolution in our focus area during a freezing cycle from (a) Oct 16th to (q) Nov 1st, 2022.

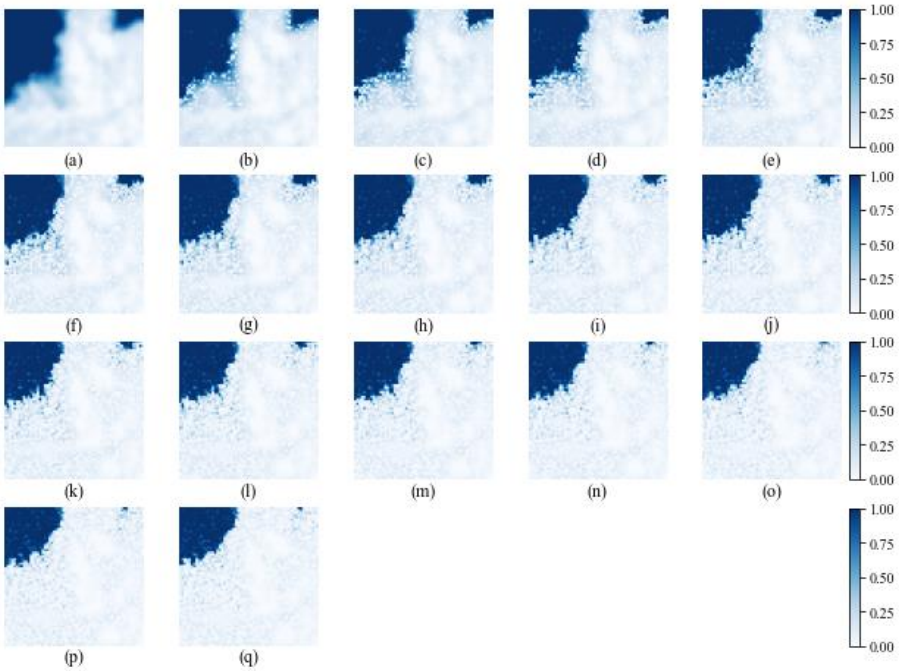

Figure 10: The simulated daily sea ice evolution, based on the semi-month Ising parameters, in our focus area during a freezing cycle from (a) Oct 16th to (q) Nov 1st, 2022.

C. Simulation results for 2023

2023 has witnessed the hottest year on record [3] [39] and is therefore a critical year for our study. Figure 11 shows the observed semi-monthly sea ice evolution from June 16th to Jan 1st in 2024 for our focus area.

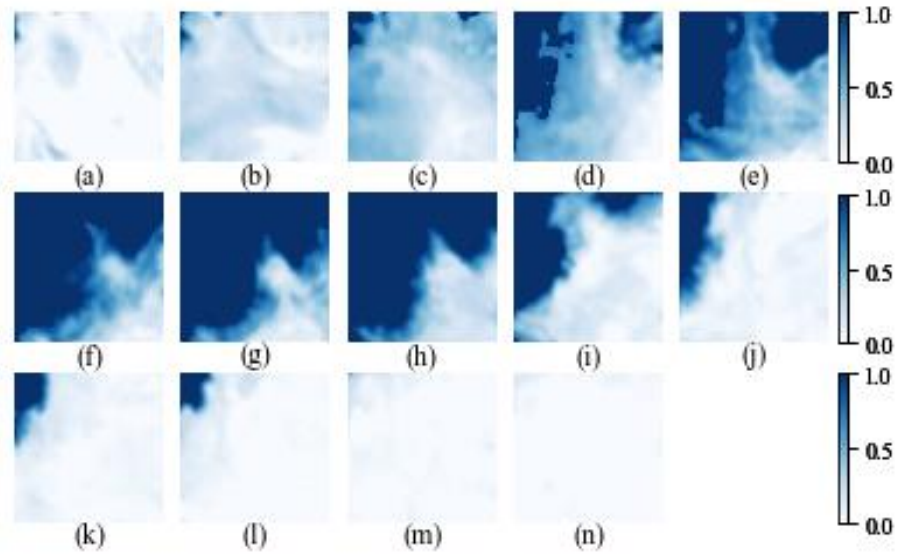

Figure 11: The actual semi-monthly sea ice evolution in our focus area in 2023: (a) June 16th, (b) July 1st, (c) July 16th, (d) Aug 1st, (e) Aug 16th, (f) Sept 1st, (g) Sept 16th, (h) Oct 1st, (i) Oct 16th, (j) Nov 1st, (k) Nov 16th, (l) Dec 1st, (m) Dec 16th, and (n) Jan 1st, 2024

Following the same practice as in Section V.A, IM simulations are conducted for 2023. The best-fit Ising parameters are shown in Table 2, the simulated configurations in Figure 12, and the comparisons for the ice coverage percentage and the ice extent in Figure 13. Consistent with the 2022 results, excellent match is observed between the IM simulation and the actual sea ice evolution. It is also worth noting that the simulated sea ice extent drops to nearly 30% in Sept 2023 in our focus area, much lower than the September 2022 level in Figure 6.

	6/16 to 7/1	**7/1 to 7/16**	**7/16 to 8/1**	**8/1 to 8/16**	**8/16 to 9/1**	**9/1 to 9/16**	**9/16 to 10/1**	**10/1 to 10/16**	**10/16 to 11/1**	**11/1 to 11/16**	**11/16 to 12/1**	**12/1 to 12/16**	**12/16 to 1/1/2024**
J	2.3	2.3	2.4	2.3	2.3	2.6	2.3	2.7	2.5	2.7	2.4	2.7	2.7
B_0	7.5	7.2	5.2	6.0	7.5	2.6	-1.0	-14.9	-14.7	-12.9	-13.8	-14.7	-15.0
B_x	-0.4	-2.0	-6.7	-7.3	-9.3	-7.3	2.5	-9.5	-4.7	-9.6	-9.3	9.3	-0.3
B_y	-2.0	-3.9	-8.0	5.2	-6.1	-1.8	-9.8	-7.9	-6.3	4.0	-2.4	-3.2	-4.8
I	10.0	10.9	10.8	11.0	10.8	11.0	11.0	10.0	9.5	10.5	9.5	10.5	10.9

Table 2: The best-fit Ising parameters for the 2023 sea ice evolution.

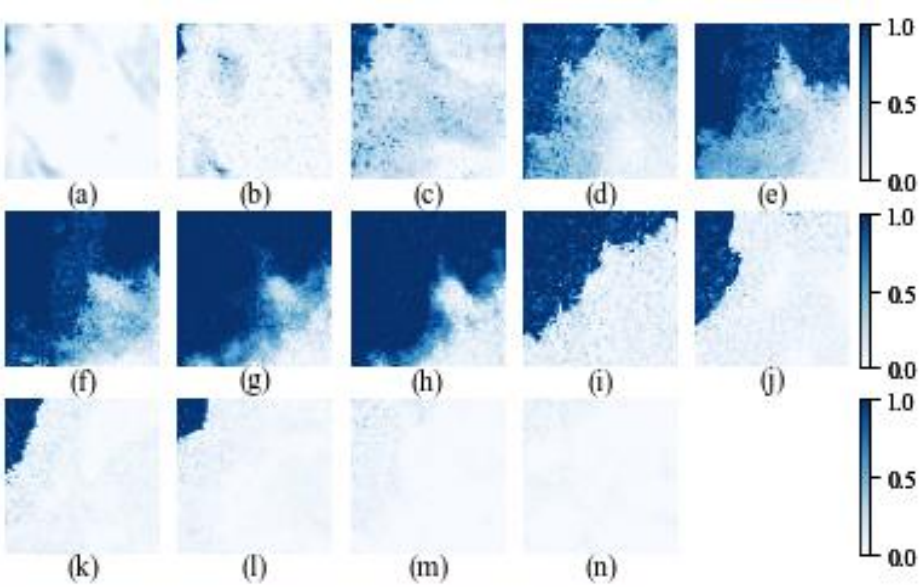

Figure 12: The simulated semi-monthly sea ice evolution in our focus area in 2023. (a) is the actual image on June 16th as the start state; (b) - (l) are simulated images on (b) July 1st, (c) July 16th, (d) Aug 1st, (e) Aug 16th, (f) Sept 1st, (g) Sept 16th, (h) Oct 1st, (i) Oct 16th, (j) Nov 1st, (k) Nov 16th, (l) Dec 1st, (m) Dec 16th, and (n) Jan 1st, 2024

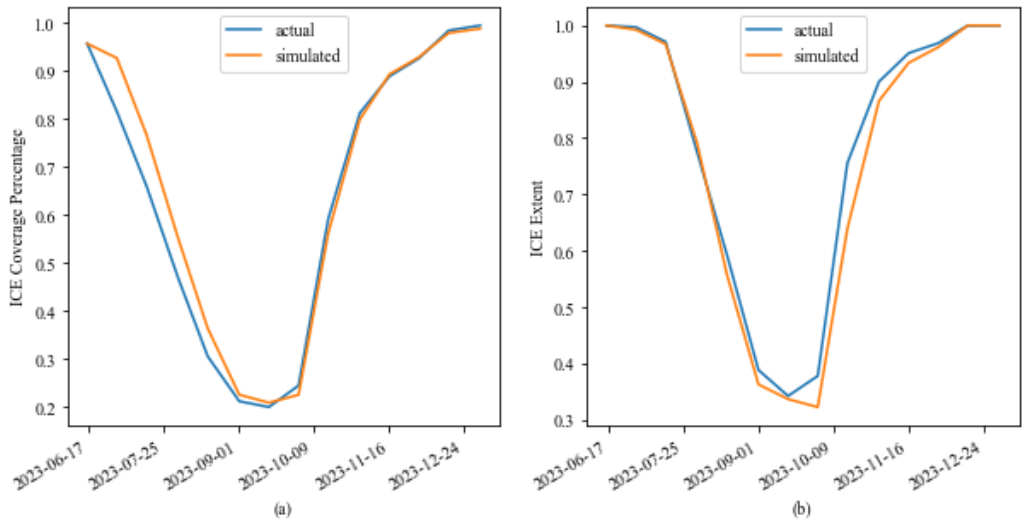

Figure 13: (a) The ice coverage percentage (the average of ice coverages) in our focus area from June 16th to Dec 1st, 2023; (b) The sea ice extent (the percentage of areas with at least 15% ice coverage) for the same period. Blue curves are the actual measures from the NRTSI data; orange ones show the IM simulation results.

D. Ice extent comparison between 2023 and 2012

2012 recorded the lowest September Arctic sea ice extent in history [2], while 2023 witnessed the hottest July and proves to be the hottest year [3] [39]. It would be an interesting experiment to compare the 2023 ice extent to that in 2012.

Following the same steps as in Section V.A and Section V.C, the IM simulations are conducted for the period of June 16th, 2012 to Jan 1st, 2013 for the focus area. To keep the paper concise, we will skip the semi-monthly actual and simulated images and the best-fit parameters, which will be provided by the author upon reasonable request. The more informative ice coverage and extent comparison charts are nevertheless included in Figure 14.

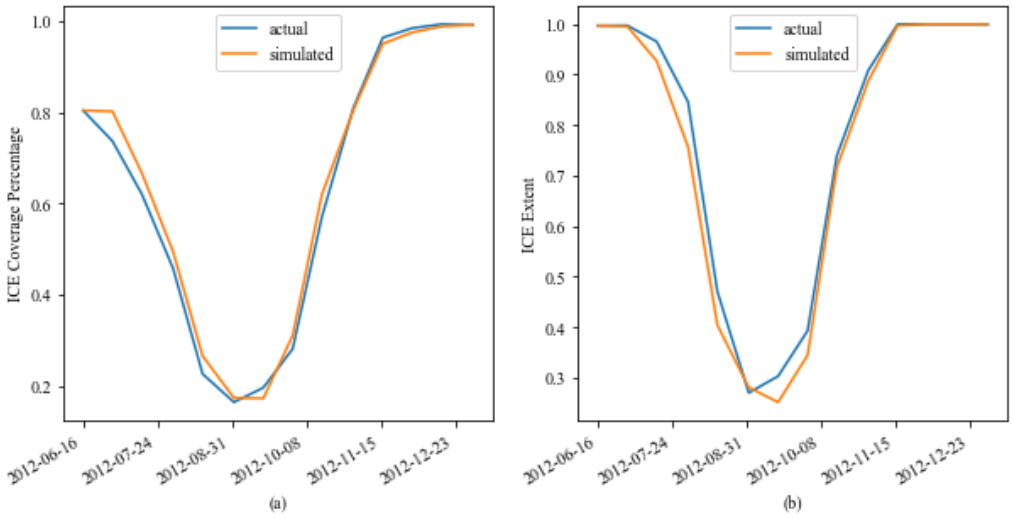

Figure 14: (a) The average ice coverage percentage in our focus area from June 16th, 2012 to Jan 1st, 2013; (b) The sea ice extent (the percentage of areas with at least 15% ice coverage) for the same period. Blue curves are the actual measures from the NRTSI data; orange ones show the IM simulation results.

Comparing Figure 13 with Figure 14 indicates that 2023 did not break the record-low Arctic sea ice extent level set in 2012, validated by both the actual measures and the IM simulations. However, 2023 sets the second lowest ice extent for our focus area, below those low levels previously achieved in 2019 and 2020[1] (2019 and 2020 results are not included in this paper but can be provided upon request.) Even though 2023 does not break the historical record, it offers no reason for us to be optimistic about the future. In fact, in the 45-year-satellite record from 1979 to 2023, 17 of the lowest minimums have all occurred in the last 17 years [47]. Many scientists are concerned that the effect of Arctic sea ice decline on global warming will intensify as the sea ice loss continues [48] [49]. Although predicting the ice extent for the future years is beyond the scope of our current study, we will discuss the possibilities in the next section.

VI. Discussion and future work

In this paper, we introduce continuous spin values and an inertia factor to a classical 2-D IM, and utilize this generalized model simulate the dynamics of the sea ice evolution in the Arctic region by employing the Metropolis-Hastings algorithm. Our results show excellent similarity with the actual sea ice dynamics, based on the ice configurations and the numerical measures including the ice coverage

[1] For the entire Arctic region not limited to our focus area, 2023 marks the 6th-lowest ice extent in history [47]; all 6 minimums are well within small margins.

percentage and the ice extent, and therefore unleash the potential of the 100-year-old classical Ising model in climate change research and other interdisciplinary science studies.

A. Discussions on the methodology

The extrapolation ability of our generalized model is worth discussing. In other words, how does the model perform if the Ising parameters fitted from one year are applied to the data of another year? For this purpose, we conduct projection of sea ice evolution from September to December 2023 based on the 2022 best-fit parameters in Table 1 for the same time periods with the initial ice image on August 16th, 2023. Our projection displays larger discrepancies from the actual images compared to Figure 12, since the idiosyncratic intra-year configurations are hard to be reproduced by the Ising parameters from a different year. However, even though the extrapolation ability of the Ising parameters is far from being perfect, the ice extent metrics calculated from our experiment accurately predicts that September 2023 would record the second lowest ice extent in history for our focus area.

The impact of the inertia factor *I* on the performance of our model is also worth discussing. In fact, we have explored the vanilla Ising model without the inertia term; the subsequent simulation results substantially underperform the results with the inertia term incorporated. This finding validates the significant strength of the inertia factor in sea ice modeling, indicating that Arctic sea ice and water indeed display the tendency to stay unchanged. However, our finding does not confirm that the inertia factor is a must-have; it is possible to improve the Ising model performance via other routes, e.g. by further enriching the functional forms of the external force *B*, which is out of scope of this paper.

Details of the above analyses are not included to keep our paper concise. They can be shared by the author upon reasonable request.

B. Will a "Blue Ocean Event" happen? If so, when will it be?

Arctic sea ice extent in September 2023 was near the historic minimum achieved in 2012. As the Arctic sea ice continues to shrink, will a "Blue Ocean Event" take place, i.e., will we see an "ice-free" Arctic Ocean? Some research predicts that it can happen in the 2030s [48].

Our current study will need to be extended to gain the full predictive power when utilized to answer this "Blue Ocean Event" question. As shown in Table 1 and Table 2, the best-fit IM parameters demonstrate the substantial impact of the external force factor *B*, which remains unexplored within the scope of our model. If the functional form of this external force is further enriched and linked to the actual environmental factors in climate change modeling, the IM framework may prove its strength in offering the "Ising Prediction" to answer the "Blue Ocean Event" question.

C. Quantum Ising model

Our study sets the stage for future Ising model research on sea ice evolution. Methodologically, besides the continuous spin IM, a much more complicated alternative idea to be explored in future research is the quantum Ising model (QIM), or the so-called transverse field Ising model [50] [51], by which the

continuous spin values can be modeled by the rotation of qubits in the Bloch Sphere [52]. Once quantum computers are accessible for personal usage [53], our research can be readily extended with the assistance of quantum computing in the future.

Acknowledgements

We thank the National Snow and Ice Data Center (NSIDC) and the National Aeronautics and Space Administration (NASA) for generously making the data publicly available and providing data support for this research.

We also thank Professor Joan Wang at the Xiamen University Malaysia Department of Physics, and Dr. Alyssa Shearer at Horace Mann School for their valuable guidance and support for this research.

Author Declarations

Conflict of Interest

The authors have no conflicts to disclose.

Data Availability

The Near-Real-Time DMSP SSMIS Daily Polar Gridded Sea Ice Concentrations" (NRTSI) data used in this study are publicly available on National Snow and Ice Data Center (NSIDC) website https://nsidc.org/data/nsidc-0081/versions/2. The data can also be provided from the author upon reasonable request.

References

[1] NSIDC, "Arctic sea ice news and analysis," 2021.

[2] NASA , "Arctic Sea Ice Minimum Extent," 2022.

[3] NOAA National Centers for Environmental Information, "Climate.gov," Januray 2024. [Online]. Available: https://www.climate.gov/news-features/featured-images/2023-was-warmest-year-modern-temperature-record#:~:text=The%20year%202023%20was%20the,decade%20(2014%E2%80%932023).

[4] E. Ising, "Beitrag zur Theorie des Ferromagnetismus," *Z. Phys,* vol. 31, no. 1, p. 2530258, 1925.

[5] E. Ising, Contribution to the Theory of Ferromagnetism, 1924.

[6] G. S. Sylvester and H. van Beijeren, "Phase Transitions for Continous-Spin Ising Ferromagnets," *Journal of Functional Analysis,* vol. 28, pp. 145-167, 1978.

[7] E. Bayong and H. T. Diep, "Effect of long-range interactions on the critical behavior of the continuous Ising model," *Physical Review B,* vol. 59, no. 18, p. 11919, 1999.

[8] N. Metropolis, A. W. Rosenbluth, M. N. Rosenbluth, A. H. Teller and E. Teller, "Equation of State Calculations by Fast Computing Machines," *J. Chem Phys,* vol. 21, no. 6, p. 1087, 1953.

[9] W. Meiser, J. Steward, H. Wilcox, M. Hardman and D. Scott, "Near-Real-Time DMSP SSMIS Daily Polar Gridded Sea Ice Concentrations, Version 2," NASA National Snow and Ice Data Center Distributed Active Archive Center, Boulder, Colorado USA, 2023.

[10] S. G. Brush, "History of the Lenz-Ising model," *Review of Modern Physics,* vol. 39, no. 4, p. 883, 1967.

[11] L. Onsager, "Crystal statistics. I. A two-dimensional model with an order-disorder transition," *Physical Review,* vol. 65, no. 3-4, pp. 117-149, 1944.

[12] H. A. Kramers and G. H. Wannier, "Statistics of the Two-Dimensional Ferromagnet. Part I," *Physical Review,* vol. 60, no. 3, pp. 252-262, 1941.

[13] H. A. Kramers and G. H. Wannier, "Statistics of the Two-Dimensional Ferromagnet. Part II," *Physical Review,* vol. 60, no. 3, pp. 263-176, 1941.

[14] J. Zuber and C. Itzykson, "Quantum field theory and the two-dimensional Ising model," *Physical Review D,* vol. 15, p. 2875, 1977.

[15] M. Aguilera, S. A. Moosavi and H. Shimazaki, "A unifying framework for mean-field theories," *Nature Communications,* vol. 12, p. 1197, 2021.

[16] S. Sides, P. Rikvold and M. Novotony, "Kinetic Ising model in an oscilating field: finite-size scaling at the dynamic phase transition," *Physical review letters,* vol. 81, no. 4, p. 4865, 1998.

[17] D. Stauffer, "Social applications of two-dimensional Ising models," *American Journal of Physics,* vol. 76, no. 4, pp. 470-473, 2008.

[18] C. Campajola, F. Lillo and D. Tantari, "Inference of the kinetic Ising model with heterogeneous missing data," *Physical Review E,* vol. 99, no. 6, p. 062138, 2019.

[19] B. Dun and Y. Roudi, "Learning and inference in a nonequilibrium Ising model with hidden nodes," *Physical Review E,* vol. 87, no. 2, p. 022127, 2013.

[20] N. N. Vtyurina, D. Dulin, M. W. Docter, A. S. Meyer, N. H. Dekker and E. A. Abbondanzieri, "Hysteresis in DNA compaction by Dps is described by an Ising model," *Proceedings of the National Academy of Sciences,* vol. 113, no. 18, pp. 4982-4987, 2016.

[21] J. Majewski, H. Li and J. Ott, "The Ising model in physics and statistical genetics," *The American Journal of Human Genetics,* vol. 69, no. 4, pp. 853-862, 2001.

[22] A. Witoelar and Y. Roudi, "Neural network reconstruction using kinetic Ising models with memory," *BMC Neurosci.,* vol. 12, p. 274, 2011.

[23] C. Donner and M. Opper, "Inverse Ising problem in continuous time: a latent variable approach," *Physical Review E,* vol. 96, p. 061104, 2017.

[24] J. Hertz, Y. Roudi and J. Tyrcha, "Ising model for inferring network structure from spike data," *arXiv.1106.1752,* 2011.

[25] Y. Roudi, D. B. and J. Hertz, "Multi-neuronal activity and functional connectivity in cell assemblies," *Curr. Opin. Neurobiol,* vol. 32, p. 38, 2015.

[26] Y. Shi and T. Duke, "Cooperative model of bacteril sensing," *Physical Review E,* vol. 58, no. 5, pp. 6399-6406, 1998.

[27] T. F. Stepinski, "Spatially explicit simulation of deforestation using the Ising-like neutral model," *Environmental Research: Ecology,* vol. 2, no. 2, p. 025003, 2023.

[28] T. F. Stepinski and J. Nowosad, "The kinetic Ising model encapsulates essential dynamics of land pattern change," *Royal Society Open Science,* vol. 10, no. 10, p. 231005, 2023.

[29] Y.-P. Ma, I. Sudakov, C. Strong and K. Golden, "Ising model for melt ponds on Arctic sea ice," *New Journal of Physics,* vol. 21, p. 063029, 2019.

[30] T. C. Schelling, "Dynamic models of segregation," *J. Math. Sociol.,* vol. 1, pp. 143-186, 1971.

[31] J. P. Bouchaud, "Crises and collective socio-economic phenomena: simple," *J. Stat. Phys.,* vol. 151, p. 567, 2013.

[32] S. Bornholdt and F. Wagner, "Stability of money: phase transitions," *Physica A: Statistical Mechanics and its Applications,* vol. 316, no. 1-4, pp. 453-468, 2002.

[33] United States Environmental Protection Agency, "Climate Change Indicators: Arctic Sea Ice," 2021. [Online]. Available: https://www.epa.gov/climate-indicators/climate-change-indicators-arctic-sea-ice#:~:text=September%20is%20typically%20when%20the,maximum%20extent%20after%20winter%20freezing..

[34] R. Lindsey and M. Scott, "Climate Change: Arctic sea ice summer minimum," *Climate.gov,* 2022.

[35] NASA Langley Research Center's Atmospheric Science Data Center, "Ice-Albedo Feedback in the Arctic," *NASA,* 2020.

[36] K. L. Oakley, M. E. Whalen, D. C. Douglas, M. S. Udevitz, T. C. Atwood and C. Jay, "Polar bear and walrus response to the rapid decline in Arctic sea ice," USGS - Science for a changing world, 2012. [Online]. Available: https://pubs.usgs.gov/publication/fs20123131.

[37] NSIDC, "EASE-Grid sea ice age, version 4," 2021.

[38] World Meteorological Organization, "Copernicus confirms July 2023 was the hottest month ever recorded," 2023.

[39] Copernius, "Record warm November consolidates 2023 as the warmest year," 2023. [Online]. Available: https://climate.copernicus.eu/record-warm-november-consolidates-2023-warmest-year#:~:text=The%20extraordinary%20global%20November%20temperatures,Climate%20Change%20Service%20(C3S).

[40] L. Boltzmann, "Studies on the balance of living force between moving material points," *Wiener Berichte,* vol. 58, pp. 517-560, 1868.

[41] A. Shekaari and M. Jafari, "Theory and simulation of the Ising model," *arXiv,* 2021.

[42] M. Krasnytska, B. Berche, Y. Holovatch and R. Kenna, "Ising model with variable spin/agent strengths," *Journal of Physics: Complexity,* vol. 1, p. 035008, 2020.

[43] Y. Hu, R. M. Horton, M. Song and J. Liu, "Reducing spread in climate model projections of a September ice-free Arctic," *Proceedings of the National Academy of Sciences,* vol. 110, no. 31, p. 12571–12576, 2013.

[44] G. J. Roy, "Time-Dependent Statistics of the Ising Model," *Journal of Mathematical Physics,* vol. 4, no. 2, pp. 294-307, 1963.

[45] C. Tsallis and D. Stariolo, "Generalized Simulated Annealing," *Physica A,* vol. 233, pp. 395-406, 1996.

[46] Y. Xiang, D. Sun, W. Fan and X. Gong, "Generalized Simulated Annealing Algorithm and Its Application to the Thomson Model," *Physics Letters A,* vol. 233, pp. 216-220, 1997.

[47] "Arctic sea ice minimum at sixth lowest extent on record," National Snow & Ice Data Center,, 2023. [Online]. Available: https://nsidc.org/arcticseaicenews/2023/09/arctic-sea-ice-minimum-at-sixth/.

[48] Y.-H. Kim, S.-K. Min, N. P. Gillett, D. Notz and E. Malinina, "Observationally-constrained projections of an ice-free Arctic even under a low emission scenario," *Nature Communications,* vol. 14, p. 3139, 2023.

[49] G. Peng, J. L. Matthews, M. Wang, R. Vose and L. Sun, "What Do Global Climate Models Tell Us about Future Arctic Sea Ice Coverage Changes?," *Climate,* vol. 8, no. 15, p. 1, 2020.

[50] P. Pferty, "The one-dimensional Ising model with a transverse field," *Annals of Physics,* pp. 79-90, 1970.

[51] B. K. Chakrabarti, A. Dutta and P. Sen, Quantum Ising Phases and Transitions in Transverse Ising Models, Berlin: Springer, 1996.

[52] M. A. Nielsen and I. L. Chuang, Quantum Computation and Quantum Information, Cambridge University Press, 2004.

[53] M. I. Dyakonov, Will We Ever Have a Quantum Computer?, Springer, 2020.